Terahertz wave generation by plasmonic-enhanced difference-frequency generation

Yuanxun Ge,[1] Jianjun Cao,[1] Zhenhua Shen,[1] Yuanlin Zheng,[1] Xianfeng Chen,[1] and Wenjie Wan[1,2,*]

[1]*Department of Physics, The State Key Laboratory of Advanced Optical Communication Systems and Networks,*
Shanghai Jiao Tong University, Shanghai 200240, China
[2]*University of Michigan–Shanghai Jiao Tong University Joint Institute,*
Shanghai Jiao Tong University, Shanghai 200240, China
*Corresponding author: wenjie.wan@sjtu.edu.cn

We propose an efficient and compact plasmonic surface-enhanced terahertz generation scheme based on nonlinear difference-frequency generation inside a metal–insulator–metal structure. Gold nanowire arrays are planted on top of the surface of a lithium niobate (LN) substrate with second-order nonlinearity to enhance both the nonlinear wavelength conversion and waveguide terahertz waves at the same time. Our numerical simulations show that our structures are capable of generating both tunable continuous and ultrafast-pulsed terahertz sources. We also discuss further improvements on the conversion efficiency by combining with Ti-diffusing LN waveguides.   © 2014 Optical Society of America

  OCIS codes: (190.4410) Nonlinear optics, parametric processes; (190.4223) Nonlinear wave mixing; (240.6680) Surface plasmons.

http://dx.doi.org/10.1364/JOSAB.31.001533

1. INTRODUCTION

The terahertz (THz) radiation, which is generally referred to as the frequency from 0.1 to 10 THz, has recently drawn much attention due to its tremendous potential applications, such as time-domain THz spectroscopy, imaging, security inspections, communications and information technology, and astronomical observation [1–5]. However, THz sources are still the limiting factors in terms of power, tunability, and cost. Currently, there are three major approaches for THz-wave generation [6]. The first kind is based on a high-speed solid-state electronic device which can provide high-power broadly tunable THz radiation; however, such devices generate THz waves on a low-frequency regime [7]. The second kind of THz-wave source is the THz quantum cascade laser (QCL). It is developing steadily, but currently it still requires low operational temperature [8,9]. The last one is through optical methods that are widely used for their convenience and flexibility.

Optical generation of THz waves falls into two general categories: one is to generate an ultrafast-pulsed THz in a photoconductive antenna [10], semiconductor [11], or optical-induced plasma [12]. The other way involves using nonlinear optical effects, such as difference-frequency generation (DFG)[13], optical rectification [14], or optical parametric oscillation [15]. Both of these methods utilize the good merits of ultrafast pulsing, high power, and wide tunability from the latest laser technologies to generate THz waves. In comparison, electronic methods—for example, semiconductor sources such as GaAs- or InGaAs/InP-based THz emitters—are already widely used in low-frequency regimes [10]. However, the low carrier lifetime of semiconductor materials limits the output THz wave to low frequency if it remains high output power, and frequency beyond 1 THz can reach only few microwatts.

Further improvement will require cryogenic cooling like with QCL technology [10]. In contrast, optical techniques for THz generation will benefit from laser technologies to flexibly develop high power, wide tunability, narrow linewidth or ultrafast-pulsed THz sources for specific applications like ultrafast spectroscopy, imaging, gas/biosensing, and so on.

THz generation by nonlinear optics is a promising approach for its simplicity, wide tunability, and capability of generating high-power Thz waves/pulse. DFG especially is popular for THz generation in a range from 1 to 10 THz. Nonlinear crystals, such as lithium niobate (LN) are well suited for THz generation, since they have large second-order nonlinear coefficient, high transparency in optical windows, and mature growing technology, which can make the generation of THz convenient and cost efficient. However, large phase mismatching between pump and THz wave and high absorption in the THz region greatly limit the conversion efficiency [15]. Several methods have been made to address these problems, such as prism coupling array for surface THz emitter, periodically poling LN crystals to satisfy the quasi-phase-matching condition, and cavity-enhanced DFG [15–18]. Currently these methods still have limited THz output on a microwatt level and relativity low conversion efficiency compared to frequency conversion at optical wavelength.

Recently, significant efforts have been devoted to surface plasmon and plasmonic structures on metallic nanostructure [19]. Surface enhancement through plasmonic structures is an important and attractive new alternative to improve the optical nonlinear process [19,20], e.g., in surface-enhanced Raman scattering. A Raman signal can be improved as high as 10^{11} simply by the plasmonic effect [21]. On the other hand, a metallic nanostructure can also serve as waveguide for

THz waves [22,23]. In this paper, we propose a new hybrid structure combining gold metal–insulator–metal (MIM) nanostructures and a nonlinear LN crystal as an efficient DFG THz source with high conversion efficiency, wide tunability, and room temperature operation. The system is based on surface plasmonic-enhanced DFG by a metallic nanostructure on the surface of a nonlinear LN crystal. At the same time, the THz wave generated by the DFG will be instantly coupled out of the LN crystal by the same metallic nanostructure as a waveguide to avoid the high absorption in the LN crystal. We numerically demonstrate a typical THz source with LN substrate and gold nanowire arrays by the finite-difference time-domain (FDTD) method. We show that high conversion efficiency and broadband tunability are possible with optimized design of such hybrid nanostructures. Our numerical results show our structures are capable of generating both continuous and ultrafast-pulsed THz sources. We also discuss further improvements on the conversion efficiency by combining with Ti-diffusing LN waveguides.

2. DESIGN OF THz SOURCE BY PLASMONIC-ENHANCED DFG

The proposed hybrid structure for THz-waves generation is shown in Fig. 1. A LN crystal substrate provides the necessary optical nonlinearity for the DFG process. On the surface of the crystal, gold nanowire arrays are planted with designed width and gap distance. The two incident lasers, both plane waves with frequency around 1550 nm for DFG, collinearly enter the LN crystal from the sidewall with direction parallel to the gold nanowire arrays with air gap as MIM structures, and they should be close to the surface to have better coupling with the gold nanowire arrays.

In the traditional DFG process, the frequency of the two incident lights and the THz wave should satisfy $\omega_t = \omega_1 - \omega_2$, where ω_t is the THz wave. Meanwhile, the phase matching condition requires

$$\frac{n_t \omega_t}{c} = \frac{n_1 \omega_1}{c} - \frac{n_2 \omega_2}{c}. \tag{1}$$

Hence, the phase mismatch is then given by

$$\Delta k = k_1 - k_2 - k_t = (n_1 \omega_1 - n_2 \omega_2 - n_t \omega_t)/c. \tag{2}$$

In bulk LN crystal, since the frequencies of the two pumping incident lights are very close to each other, the dispersion relation of 1550 nm light inside the LN crystal is relatively flat, but the effective refractive index of THz wave differs a lot from the incident light of the infrared [24]. For example, in a bulk MgO:LiNbO$_3$ crystal, the refractive index of the incident light is about 2.15 and for THz it is about 5.2. In order to phase match these two frequency regions, one major scheme is to utilize the Čherenkov phase-matching condition, where the velocity of the pumping waves inside the nonlinear crystal is greater than the velocity of the radiated wave (THz waves) [25]. The radiation angle θ is given by

$$\cos \theta = n_{\text{optical}}/n_{\text{THz}}, \tag{3}$$

where n_{optical}, is the refractive index of the pumping wave in the crystal, and n_{THz} is the refractive index of the THz wave in the crystal. However, in usual bulk scheme, these THz waves still require a prism coupler in order to be out-coupled of LN crystals due to the total internal reflection condition.

In our design, DFG occurs at the junction between the LN crystal and gold nanowires. The gold nanowire arrays on the surface of the LN crystal serve as MIM waveguides where generated THz waves can propagate by surface plasmonic mode, as Fig. 1(b) shows. More importantly, such MIM structure can also plasmonic-enhance the optical fields at the infrared to improve the nonlinear DFG. Recent works indicate that the fundamental symmetric mode will always exist in the MIM waveguide at any frequency range [26,27]; this guarantees the coexistence of waveguiding for both optical and THz waves. Figure 1(d) shows the hybrid plasmonic mode for optical surface waves at the junction between the MIM and LN crystal surface. The highest peak power can be enhanced as high as 20 times. In contrast, the surface plasmon mode for THz waves is more confined inside MIM. The overlapping area between these two modes is rather small, indicating that MIM can perform as a sole waveguide without coherent interference with the optical mode affecting the DFG conversion. A MIM THz waveguide can be an alternative to a prism coupler in the Čherenkov phase-matched DFG.

We calculate dispersion relations of the MIM waveguide for both the THz and optical regions, as shown in Fig. 2. We can see that for a DFG process, the effective refraction index of THz waves is larger than that of optical waves. The Čherenkov
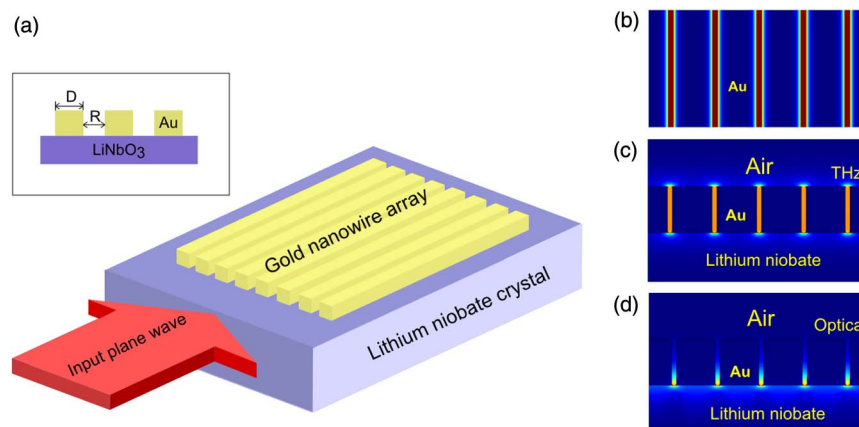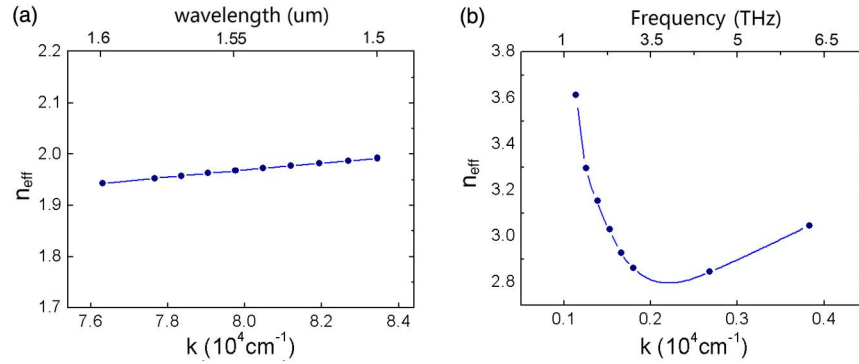

Fig. 1.   (a) Schematics of the proposed THz source with a metal–insulator–metal on top of LN crystal, (b) top-view of optical waveguide mode and the cross-section fundamental modes for (c) THz (d) optical.

Fig. 2.   (a) Dispersion relation of the metal–insulator–metal waveguides with 400 nm width, 500 nm height, and 50 nm separation for wavelength between 1500 and 1600 nm. (b) Dispersion relation of such structure on THz region.

phase-matching scheme still apply, i.e., optical waves travel faster than THz waves. The generated THz waves can immediately be coupled out into a MIM waveguide. This coupling can be greatly affected by the nanowire's geometry structure, e.g., height, width and gap distance, which we will explore later in the paper. On the other hand, the gold nanowire array enhances the optical field inside the gap to increase the efficiency of the DFG process. Hence, we have to carefully design the structure to maximize the output THz waves. More interestingly, as dispersion relations in Fig. 2 shows, the effective index difference between the optical waves and THz waves diminishes compared to that in the bulk. This trend may enable tailoring of the MIM plasmonic structure for a novel phase-matching scheme through waveguide dispersion management, which requires further investigation.

3. PLASMONIC-ENHANCED THz SOURCE: NUMERICAL SIMULATION

We now illustrate the ability of the proposed device to generate THz waves by DFG process by 3D FDTD numerical simulation [28]. In our simulation, the optical nonlinear crystal is LN, which has 5.5 μm thickness. The metal is modeled as gold material using a Drude model (optical loss has been considered). The width D of the metal nanowires is set to be 400 nm and the separation between the metal nanowires is 50 nm, while the propagation length is set to 4 μm, which is shorter than the coherence length of two incident lights ($L_c = \pi/\Delta k, \Delta k = k_1 - k_2$). In our calculation, the targeted THz waves are between 1–5 THz. One input light is fixed at a wavelength of 1550 nm, the other one is varied between 1510.94–1538.07 nm. According the dispersion curve in

Fig. 2(a), we calculate the coherence length to be around 13.24–44.13 μm, longer than our designed propagation length; this not only ensures the monotonic growth of THz waves, but reduces the loss factors during the propagation of infrared lights inside MIM waveguides.

We first consider the continuous wave (CW) situation that the incident lights are two CW laser sources. The wavelengths of the two lights are 1550 and 1526.34 nm, which will generate a 3 THz output by the DFG process. The calculated THz output power together with a quadratic fit of THz wave versus the input power is shown in Fig. 3(a). It is obvious that the nanostructure can greatly enhance the THz output. We can also see that the quadratic fit agrees well with the data and thus the quadratic scaling can be expected for a DFG process [29]. In particular, the THz generator can provide CW output up to 0.2 mW with about 10 W input power. The conversion efficiency is about 10^{-5}, which is close to the efficiency of DFG by pulse laser [25]. Since high-power CW 1550 nm lasers (more than 30 W output) have been developed rapidly using fiber laser, we expect that our design is capable of producing CW tunable THz waves on milliwatt level in such a manner.

To study the characteristic of frequency tuning, we vary the wavelength of one of the incident light around 1526.34 nm. Since there are already many THz sources in the low-frequency region, such as InGaAs/InP THz emitter, we pay more attention to the higher-frequency region (>1 THz). The wavelength of the incident light is set in a range between 1512.47 and 1542.03 nm to obtain the desired THz-wave outputs in the frequency range from 1 to 4.8 THz. The tuning output characteristic of the THz generator is shown in Fig. 3(b). As shown, the output spectrum of THz wave is relatively flat
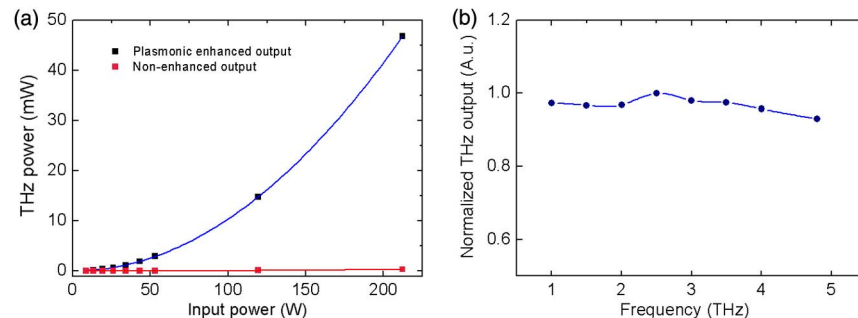

Fig. 3.   (a) CW THz output power with a quadratic fit of THz wave versus the input power. Blue line is the plasmonic MIM-enhanced setup and red line is nonenhanced one. (b) Normalized output spectrum of generated THz waves.
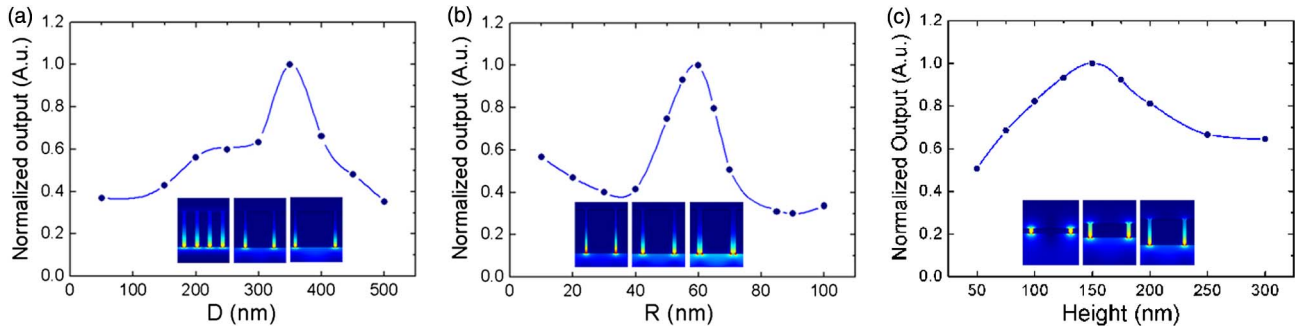
Fig. 4.   Normalized output of THz wave versus (a) the width of the gold nanowires D (b) the separation of the gold nanowires R and (c) the height of the gold nanowires. Optical modes of 100, 350, 500 nm waveguide widths, 50 nm gap, and 400 nm height are shown in (a) insets. Optical modes of 40, 60, 80 nm gap, 350 nm width, and 400 nm height are shown in (b) insets. Optical modes of 50, 150, 300 nm waveguide heights, 50 nm gap, and 350 nm width are shown in (c) insets.

over a wide range from 1 to 4.8 THz. This indicates our proposed setup may be useful as a widely tunable continuous THz wave source.

In order to optimize our design for better conversion efficiency, we also calculate the output of the THz generator by varying structure parameters D and R. Figure 4(a) shows the dependence of the output and the width D of the gold nanowire. The separation of the nanowire is fixed at 50 nm. We can see that the output power reaches its maximum value with 350 nm width. When the width D is fixed at 350 nm, an output peak appears around 60 nm in Fig. 4(b) when varying the gap R; however, a relatively weak peak around 150 nm height in Fig. 4(c) shows up when varying the height H of nanowires. Two major factors are considered during this DFG process near the MIM and LN crystal surface: (1) MIM waveguide's plasmonic enhancement. As the most enhanced optical field occurs insides the MIM gap near the LN surface, by varying the waveguide's width and gap, we effectively change the number of gaps [see Fig. 4(a) inset]. Also the gap's size affects the enhancement factors. For example, an optical field inside a 40 nm gap size is much stronger than that of an 80 nm gap in Fig. 4(b). (2) THz waves out-coupling efficiency. Though we show that THz waves are well confined inside the MIM waveguides in Fig. 1, the width of these nanowires is much smaller compared to THz waves. Hence, the nearest sites' coupling may occur in this case, as we mention earlier; this will require us to do further study on tailoring the MIM's dispersion for better outcoupling.

We also consider using our nanostructure for ultrafast-pulsed THz generation similar to a bowtie antenna type THz source [10]. We choose one input femtosecond laser with 100 fs pulse width, 80 nm spectrum range, and 1560 nm center

wavelength; the repetition rate of the laser is 80 MHz and the average output power is 350 mW. The output characteristics of our generator are shown in Fig. 5, which shows both the temporal waveform of the THz output and the THz power spectra. We can see that for a femtosecond pulse input, the generator gives a THz pulse output which has a picosecond scale width. The output THz pulse has a peak power of 58 W. The average THz output of this system is calculated as 1.86 mW, and we get an extremely high conversion efficiency of 0.531%, which is much higher than that from other works, e.g., a LN crystal with 0.1% efficiency [30], backward pulse from multiperiod periodically poled LN with 0.16% efficiency [31,32].

In order to improve conversion efficiency further, we consider combining our hybrid MIM nanostructure with a Ti-diffused LN waveguide. A Ti-diffused LN waveguide can further concentrate the light inside the Ti-diffused waveguide area, as shown in Fig. 6(a). The gold nanowire arrays are placed on the surface of the Ti-diffused waveguide region. The Ti-diffused region has a refractive index about 1.09×10^{-3} higher than the rest of the regions waveguiding the incident light to this area. This further concentration of light directly improves the output conversion efficiency, as shown in Fig. 6(b): the Ti-diffused setup has significantly higher output around 8.5 mW with 53 W pumping powers, which is nearly 3 times larger than that of the nondiffused system. Clearly, Ti-diffused configurations are an even more effective THz source. It is worth mentioning that we are not limited to a waveguiding structure; other photonic nanostructures like 2D photonic crystal, slow-light plasmonic gratings [33] can enhance light field and can all be integrated with our design. However, these 2D geometries usually attempt to localize
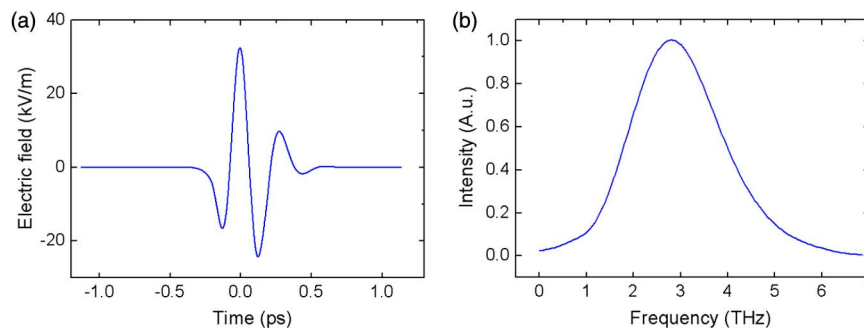

Fig. 5.   (a) Temporal waveform of the THz wave pulse. (b) THz power spectra.
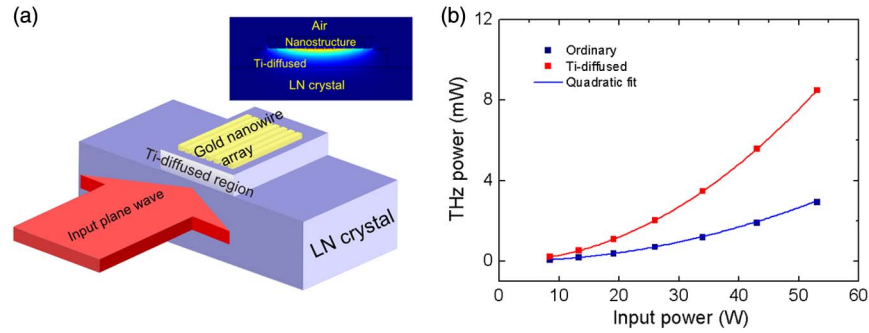
Fig. 6. (a) Schematics of the improved THz generator nanostructure with Ti-diffused LN waveguide. (b) Output characteristics of the Ti-diffused configuration and compared with the nondiffused setup. Both the outputs are quadratic fitted. The parameters of the nanostructure are 50 nm for R and 400 nm for D.

the optical field instead of propagating them, reducing the THz output. This requires further investigation.

At last, we would like to comment on possible experimental realizations for the current design. For the device fabrication, the smallest feature size in our design is around 50 nm, which is achievable with the current nanofabrication, especially using nanoimprint techniques for large area devices. For the optical experiment, one main obstacle is the coupling scheme: here we have already shown that normal incident launch with Gaussian beams can simply excite both optical and THz modes inside the MIM structures, much easier compared to the prism coupling scheme [30]. However, some factors such as phase-lock of two input lasers, input laser coupling, and LN crystal temperature control, may affect the final conversion efficiency. All of these problems have a mature solution in the nonlinear optics community, hence we expect our design can be implemented quickly in our future study.

4. CONCLUSION

We have proposed a THz generation scheme based on nonlinear DFG near a MIM on top of a second-order nonlinear crystal. Our numerical results demonstrate potentially better conversion efficiency over some traditional THz generation methods for both continuous and ultrafast-pulsed sources. We expect our design can be beneficial for an efficient and compact THz source in the near future.

ACKNOWLEDGMENTS

REFERENCES

1. P. H. Siegel, "THz instruments for space," IEEE Trans. Antennas Propag. **55**, 2957–2965 (2007).
2. P. H. Siegel, "Terahertz technology," IEEE Trans. Microw. Theory Tech. **50**, 910–928 (2002).
3. B. Ferguson and X.-C. Zhang, "Materials for terahertz science and technology," Nat. Mater. **1**, 26–33 (2002).
4. K. Kawase, Y. Ogawa, Y. Watanabe, and H. Inoue, "Non-destructive terahertz imaging of illicit drugs using spectral fingerprints," Opt. Express **11**, 2549–2554 (2003).
5. E. Knoesel, M. Bonn, J. Shan, and T. Heinz, "Charge transport and carrier dynamics in liquids probed by THz time-domain spectroscopy," Phys. Rev. Lett. **86**, 340 (2001).
6. M. Tonouchi, "Cutting-edge terahertz technology," Nat. Photonics **1**, 97–105 (2007).
7. H. Ito, F. Nakajima, T. Furuta, and T. Ishibashi, "Continuous THz-wave generation using antenna-integrated uni-travelling-carrier photodiodes," Semicond. Sci. Technol. **20**, S191 (2005).
8. B. S. Williams, "Terahertz quantum-cascade lasers," Nat. Photonics **1**, 517–525 (2007).
9. S. Kumar, Q. Hu, and J. L. Reno, "186 K operation of terahertz quantum-cascade lasers based on a diagonal design," Appl. Phys. Lett. **94**, 131105 (2009).
10. S. Matsuura, M. Tani, and K. Sakai, "Generation of coherent terahertz radiation by photomixing in dipole photoconductive antennas," Appl. Phys. Lett. **70**, 559–561 (1997).
11. P. U. Jepsen, R. Jacobsen, and S. Keiding, "Generation and detection of terahertz pulses from biased semiconductor antennas," J. Opt. Soc. Am. B **13**, 2424–2436 (1996).
12. J. Dai, X. Xie, and X. C. Zhang, "Detection of broadband terahertz waves with a laser-induced plasma in gases," Phys. Rev. lett. **97**, 103903 (2006).
13. T. Wang, S. Lin, Y. Lin, A. Chiang, and Y. Huang, "Forward and backward terahertz-wave difference-frequency generations from periodically poled lithium niobate," Opt. Express **16**, 6471–6478 (2008).
14. M. C. Hoffmann, K.-L. Yeh, J. Hebling, and K. A. Nelson, "Efficient terahertz generation by optical rectification at 1035 nm," Opt. Express **15**, 11706–11713 (2007).
15. T. Ikari, X. Zhang, H. Minamide, and H. Ito, "THz-wave parametric oscillator with a surface-emitted configuration," Opt. Express **14**, 1604–1610 (2006).
16. M. Scheller, J. M. Yarborough, J. V. Moloney, M. Fallahi, M. Koch, and S. W. Koch, "Room temperature continuous wave milliwatt terahertz source," Opt. Express **18**, 27112–27117 (2010).
17. K. Suizu, K. Koketsu, T. Shibuya, T. Tsutsui, T. Akiba, and K. Kawase, "Extremely frequency-widened terahertz wave generation using Cherenkov-type radiation," Opt. Express **17**, 6676–6681 (2009).
18. W. Shi, Y. J. Ding, N. Fernelius, and K. Vodopyanov, "Efficient, tunable, and coherent 0.18–5.27-THz source based on GaSe crystal," Opt. Lett. **27**, 1454–1456 (2002).
19. W. L. Barnes, A. Dereux, and T. W. Ebbesen, "Surface plasmon subwavelength optics," Nature **424**, 824–830 (2003).
20. G. Ramakrishnan, N. Kumar, P. C. Planken, D. Tanaka, and K. Kajikawa, "Surface plasmon-enhanced terahertz emission from a hemicyanine self-assembled monolayer," Opt. Express **20**, 4067–4073 (2012).
21. B. J. Evan, L. R. C. Eric, M. Matthias, and E. G. Pablo, "Surface enhanced Raman scattering enhancement factors: a comprehensive study," J. Phys. Chem. C **111**, 13794–13803 (2007).
22. C. R. Williams, S. R. Andrews, S. Maier, A. Fernández-Domínguez, L. Martín-Moreno, and F. García-Vidal, "Highly confined guiding of terahertz surface plasmon polaritons on structured metal surfaces," Nat. Photonics **2**, 175–179 (2008).
23. Q. Gan, Z. Fu, Y. J. Ding, and F. J. Bartoli, "Ultrawide-bandwidth slow-light system based on THz plasmonic graded metallic grating structures," Phys. Rev. Lett. **100**, 256803 (2008).
24. D. Bosomworth, "The far infrared optical properties of $LiNbO_3$," Appl. Phys. Lett. **9**, 330–331 (1966).

25. K. Suizu, T. Shibuya, T. Akiba, T. Tutui, C. Otani, and K. Kawase, "Čherenkov phase-matched monochromatic THz wave generation using difference frequency generation with a lithium niobate crystal," Opt. Express **16**, 7493–7498 (2008).

26. J. Park, K.-Y. Kim, I.-M. Lee, H. Na, S.-Y. Lee, and B. Lee, "Trapping light in plasmonic waveguides," Opt. Express **18**, 598–623 (2010).

27. Y. Zhang, X. Zhang, T. Mei, and M. Fiddy, "Negative index modes in surface plasmon waveguides: a study of the relations between lossless and lossy cases," Opt. Express **18**, 12213–12225 (2010).

28. Lumerical Computational Solutions Inc., "FDTD solutions," https://www.lumerical.com/tcad-products/fdtd/.

29. R. W. Boyd, *Nonlinear Optics* (Academic, 2010), Chap. 1.

30. H. Hirori, F. Blanchard, and K. Tanaka, "Single-cycle terahertz pulses with amplitudes exceeding 1 MV/cm generated by optical rectification in $LiNbO_3$," Appl. Phys. Lett. **98**, 091106 (2011).

31. G. Xu, X. Mu, Y. J. Ding, and I. B. Zotova, "Efficient generation of backward terahertz pulses from multiperiod periodically poled lithium niobate," Opt. Lett. **34**, 995–997 (2009).

32. R. Chen, G. Sun, G. Xu, Y. J. Ding, and I. B. Zotova, "Generation of high-frequency terahertz waves in periodically poled $LiNbO_3$ based on backward parametric interaction," Appl. Phys. Lett. **101**, 111101 (2012).

33. Q. Gan, Y. Gao, K. Wagner, D. Vezenov, Y. J. Ding, and F. J. Bartoli, "Experimental verification of the rainbow trapping effect in adiabatic plasmonic gratings," Proc. Natl. Acad. Sci. USA **108**, 5169–5173 (2011).